

Environmental Sensitivity of Fiber Bragg Grating Sensors for Aerospace Prognostics

Original

Environmental Sensitivity of Fiber Bragg Grating Sensors for Aerospace Prognostics / Dalla Vedova, M.D.L., Berri, P.C., Aimasso, A.. - ELETTRONICO. - (2021), pp. 1561-1567. (31st European Safety and Reliability Conference (ESREL 2021) Angers (France) 19 – 23 September 2021) [10.3850/978-981-18-2016-8_634-cd].

Availability:

This version is available at: 11583/2962007 since: 2022-04-24T09:12:38Z

Publisher:

Research Publishing Services

Published

DOI:10.3850/978-981-18-2016-8_634-cd

Terms of use:

This article is made available under terms and conditions as specified in the corresponding bibliographic description in the repository

Publisher copyright

(Article begins on next page)

Environmental sensitivity of Fiber Bragg Grating sensors for aerospace prognostics

Matteo D.L. Dalla Vedova

Dept.of Mechanical & Aerospace Engineering, Politecnico di Torino, Italy. E-mail: matteo.dallavedova@polito.it

Pier Carlo Berri

Dept.of Mechanical & Aerospace Engineering, Politecnico di Torino, Italy. E-mail: pier.berri@polito.it

Alessandro Aimasso

Dept.of Mechanical & Aerospace Engineering, Politecnico di Torino, Italy. E-mail: alessio.laudani4@gmail.com

Optical sensors have recently gained interest due to the many advantages they offer over traditional electrical sensors commonly used in aerospace applications. In particular, their total insensitivity to electromagnetic interference (EMI), the ease of multiplexing of different signals on a single line, the excellent resilience to hostile environments, the very compact dimensions, and the considerable overall weight savings resulting from the signal cables reduction, make technological solutions based on optical fibers a compelling alternative to traditional sensing elements. In this work, authors consider optical sensors based on Fiber Bragg Gratings (FBGs), which can reflect a very narrow band of wavelengths, called the Bragg wavelength, but are almost transparent for the other signals. This behaviour is obtained by realizing local variations of the refractive index of the FBG core. The Bragg wavelength, nominally defined in the production phase by the grating etching process, can vary as a function of physical changes in the sensor itself or environmental conditions (physical stresses applied to the grating or variations of temperature or humidity). The correlation of the Bragg wavelength variation with the physical variations of the sensor is essential to guarantee satisfactory levels of accuracy and reliability. In particular, using FBGs as mechanical strain sensors, it is crucial to estimate with proper accuracy the disturbance generated by environmental conditions and conceive an effective compensation method. Hence, this work studies the effects of environmental temperature and humidity variations on measurements, examining possible non-linear, time-dependent phenomena arising from the FBGs bonding. For this purpose, the authors developed a dedicated test bench to simultaneously detect the various physical measures (FBG deformation, temperature, humidity, Bragg wavelength variation), analyse their correlations, and formulate the said compensation strategy.

Keywords: Aerospace applications, FBG, fiber bonding, environmental factors sensitivity, mechanical strain, optical sensors.

1. Introduction

In aerospace, the Fault Detection and Isolation (FDI) algorithms developed for prognostics of on-board systems need to early identify the failure precursors (i.e. when the effects on system performances are still almost negligible), according to Borello et al. (2009). Therefore, it is often necessary to analyse a large of data related to the measures of the system working parameters. These sensors have to be very robust and accurate, avoiding the sensor noise to hide information necessary to estimate the components health (Byington et al. 2004). As regards the aircraft on-board systems, and in particular the Flight Control System (FCS), often FDI methods are based on either machine learning algorithms, as reported by Anderson and Aylward (1993), De Martin et al. (2019), Quattrocchi et al. (2020), or on model-based strategies, as proposed by Dalla Vedova et al. (2019), Hasan and Johansen (2018), or by their combinations, as shown by Berri et al. (2018, 2019a). However, regardless of the approach adopted, these prognostic algorithms require the acquisition of specific fault precursors which, as reported by Goebel et al. (2017), can have a significantly different nature depending on the

system and the faults considered (temperatures, currents, pressures, vibrations, torques, displacements, actuation velocity, etc.). As reported by Vachtsevanos et al. (2006), the effectiveness of the prognostic algorithm is influenced by the accuracy and repeatability of the measurements and the susceptibility of the sensors to external disturbances (e.g. electromagnetic interference, electrical noise, voltage spikes, electrostatic discharges, components thermal drift). Therefore, in different applications (eg. temperature, strain, vibration, pressure measurements), the possibility of replacing some traditional sensors with innovative types based on optical fiber Bragg grating (FBG) are currently being evaluated, as described by Kashyap (2010), Mihailov (2012) and Berri et al. (2019b). These consist of a small section of an optical glass fiber treated to be sensitive to deformation, both mechanical and thermal, as shown by Quattrocchi et al. (2021). Such sensors based on FBG are already used, in place of strain gauges or traditional thermal probes in many applications, as reported by Brusa et al. (2019), providing measurements of comparable accuracy but guaranteeing insensitivity to electromagnetic interference and good compatibility to harsh environments, as reported by Mihailov et al. (2017).

Furthermore, as evidenced by Santos and Farahi (2018), a single optical fiber can contain tens to hundreds of sensors. Therefore, it possible to obtain highly compact sensors and distributed measurement networks, avoiding the typical problems of weight and installation complexity related to individual electrical wiring and sensor signal conditioning.

However, it should be noted that, as highlighted by Tanaka et al. (2003), the FBGs measurements are significantly influenced by temperature and, albeit to a lesser extent, also by environmental humidity. In other words, as reported by Ramakrishnan et al. (2016), the FBG measures a variation of the Bragg wavelength, due simultaneously to different effects (mechanical deformation, temperature, humidity) and, at least in a first instance, it is not possible to quantify the different contributions (Adamovsky, 2012).

In case of constant temperature and humidity values (or characterized by very modest variations or with very slow temporal evolutions), their effect on the accuracy of the mechanical deformation measurements of the FBG can be assumed negligible or, at the limit, can be compensated by calibration of the sensor (Jones, 2018).

On the contrary, this approach will be less and less effective as the variations mentioned above increase (i.e. when their effect is no longer negligible compared to the mechanical deformations to be measured).

Therefore, in case of significant changes in temperature or environmental humidity, it is necessary to evaluate the effect these changes induce on the FBGs measurements and define a suitable strategy to refine the raw values provided by the optical sensors affected by such disturbances (Wang et al. 2015). Indeed, the correlation of the Bragg wavelength variation with the physical variations of the sensor is essential to guarantee satisfactory levels of accuracy and reliability.

In particular, using FBGs as mechanical strain sensors, it is crucial to estimate with proper accuracy the disturbance generated by environmental conditions and conceive an effective compensation method.

Hence, this work studies the effects of environmental temperature and humidity variations on measurements, examining possible non-linear, time-dependent phenomena arising from the FBGs bonding. For this purpose, the authors developed a dedicated test bench to simultaneously detect the various physical measures (FBG deformation, temperature, humidity, Bragg wavelength variation), analyse their correlations, and formulate the said compensation strategy.

2. Fiber Bragg Sensors applied to on-board systems

Optical sensors based on Fiber Bragg Gratings allow measurements of several heterogeneous quantities with minimal invasivity and small form factor (Krohn, 2014). The FBG is a section of an optical fiber extended for a few millimeters. A periodical modulation of its refraction index is produced through exposure to a high-power UV laser. The fiber for FBG manufacture is usually made of a germanium-doped glass: this material is photosensitive, and its refraction index can be modified by high-intensity UV radiation.

As described by Kreuzer (2006), the grating behaves as a wavelength-specific dielectric mirror: the FBG reflects a particular wavelength while the others are transmitted. The reflected wavelength λ_B is related to the grating pitch Λ and refraction index n :

$$\lambda_B = 2n_{EFF} \cdot \Lambda \quad (1)$$

The operation of FBGs is based on Fresnel reflection (Ahuja and Parande, 2012). This physical phenomenon enables the production of temperature and strain sensors. The mechanical deformation $\Delta\varepsilon$ and the temperature variation ΔT affect both the effective refractive index and the axial pitch of the fiber, modifying the reflected wavelength. Therefore, the variation of the reflected wavelength $\Delta\lambda_B$ can be expressed as follows:

$$\Delta\lambda_B = \lambda_B(1 + p_E)\Delta\varepsilon + \lambda_B(\alpha_A + \alpha_n)\Delta T \quad (2)$$

where, according to Santos (2018) and Jones (2018):

- λ_B is the nominal reflected wavelength;
- p_E is the strain-optic coefficient of the fiber;
- $\Delta\varepsilon$ is the variation of fiber strain;
- α_A is the thermal expansion coefficient of the fiber;
- α_n is the thermo-optic coefficient of the fiber;
- ΔT is the variation of the temperature.

Equation (2) can be reformulated as follows:

$$\Delta\lambda_B = K_\varepsilon\Delta\varepsilon + K_T\Delta T \quad (3)$$

where the terms K_ε and K_T are respectively defined coefficient of strain and coefficient of temperature.

The coefficients K_ε and K_T are then defined as:

$$K_\varepsilon = \lambda_B(1 + p_E) \quad (4)$$

$$K_T = \lambda_B(\alpha_A + \alpha_n) \quad (5)$$

where these coefficients are calculated for the case in which there is an optical fiber that undergoes a stress but without being glued on other materials. More in details, K_ε is function of the strain-optic coefficient: it depends from the material of the fiber and it explains the variation of the refraction index caused by a normal stress.

Generally, it has got a value of $p_E = -0,212$.

Instead, the K_T is composed by the contribute of two different sources:

- The thermo-optic coefficient: it represents the variation of the refraction index caused by the temperature. For the optical fiber it assumes a value of $\alpha_n = 5.77 \cdot 10^{-6} [1/^\circ\text{C}]$. This coefficient depends by the material that composes the fiber and so it remains constant in different applications.
- The thermal expansion coefficient represents the effect of the temperature on the physical disposition of the Bragg grating. Indeed, the variation of temperature causes a deformation of this structure and consequently the reflected wavelength undergoes a modify. In case of a fiber not glued on a support it has got the value of the thermal expansion of the glass (the material making core and cladding of the fiber). Commonly, it is assumed $\alpha_A = 0.55 \cdot 10^{-6} [1/^\circ\text{C}]$.

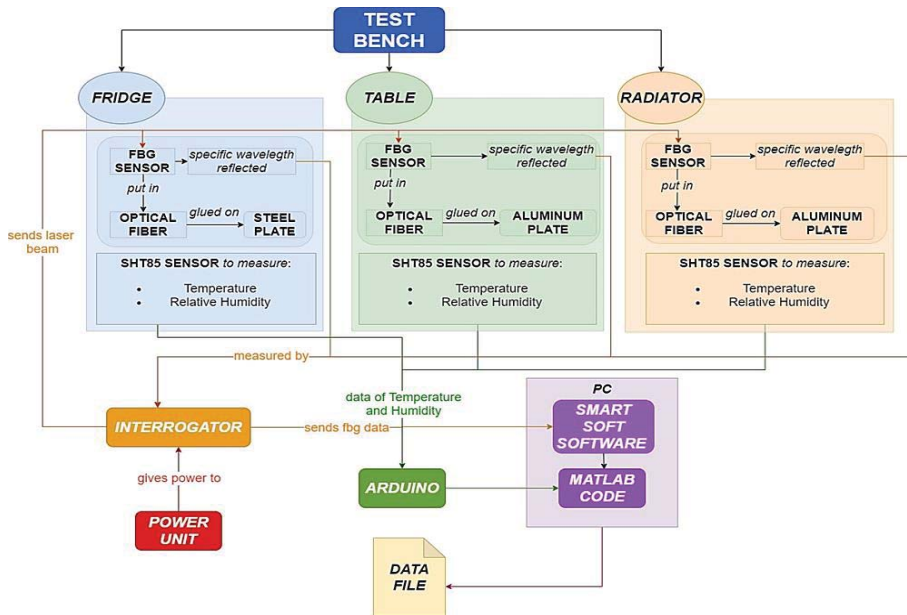


Fig. 1. Schematic representation of the general layout of the proposed FBG environmental sensitivity test-bench.

3. FBG environmental sensitivity test-bench

As previously reported, this work reports the first results of a research campaign that aims to evaluate the effects produced by changes in temperature and environmental relative humidity on the optical sensors measurements, examining possible non-linear, time-dependent phenomena deriving from FBGs bonding. To this purpose, the authors developed a test bench to simultaneously detect the various significant physical quantities (i.e. fiber strain, punctual temperature, local humidity, Bragg wavelength variation) and analyse their correlations. The results obtained will then be used to evaluate any compensation strategies.

As schematically represented in figure 1, the authors' test bench comprises three main subsystems (called "Fridge", "Table" and "Radiator"), expressly designed to test the sensors in three different operating situations (to evaluate three scenarios having different time-histories of environmental conditions) and study the response of FBGs to variable temperature and relative humidity. The main components of the test bench are:

- Three optical fibers with related FBG sensors;
- Mechanical fiber support frames;
- FBG Interrogator;
- Electrical power unit;
- SHT85 temperature and humidity sensors;
- ARDUINO UNO microcontroller;
- Personal computer (PC).

The *FBG sensors* are the main subject of this study. They are installed on three different optical fiber lines and then placed on dedicated support in each measure station. The FBGs present a nominal wavelength of 1545 nm and 1550 nm. Still, thanks to the structure of the test bench, composed of three independent optical fiber branches individually connected to three different interrogator channels, it is acceptable having two sensors with the same nominal wavelength (but installed on different branches).

The *Mechanical fiber support frames* are metal plates on which the FBGs are glued. The fibers are properly pre-tensioned using micro-handlers. The exact knowledge of the initial pre-tensioning value applied to each fiber (and, therefore, detected by the related FBG sensor) is essential to correlate the wavelength variation $\Delta\lambda_B$ with the relative strain $\Delta\varepsilon$ correctly. The bonding between fibers and related micro-handlers is performed by fixing them directed to the supports using Araldite 2011 glue. It is an epoxydic adhesive that polymerizes at environmental temperature. In this way, the glue has high resistance and excellent tenacity, resulting in suitable for undergoing loads applied for periods, both static and dynamic. The low shrinkage and the elevated shear stiffness of the glue minimize the adverse effects on the sensor measures.

The *FBG Interrogator* is a device capable of autonomously identifying and interrogating the FBGs in the fibers connected to the different channels, then collecting and analysing the responses of these sensors.

It has got a dedicated communication channel for each FBG, avoiding eventual misunderstandings about data coming from different sensors. The interrogator sends a laser beam to the fiber and detects the wavelength of the reflected signal. In this application the authors used the *SmartScan SBI* laser interrogator developed by the *Smart Fibres* society (as described by Lelli, 2020). The results shown in this work are managed by the proprietary *SmartScan* software *SmartSoft* (see www.smartfibres.com). The system operates a data acquisition loop one time per 10 minutes: each measurement has a duration of 10 seconds with a frequency of sampling of 25 kHz. All data acquired in a specific measurement on a given Bragg are averaged, obtaining the related instantaneous wavelength value. The accuracy and resolution of measures depending on the bandwidth of the laser and the postprocessing algorithms employed. Typical values are about 1 pm in wavelength, corresponding to about 1 microstrain or 0.1 K.

The *Electrical power unit* shall provide the energy to the interrogator to let it operate. It has got two output channels. The maximum output current is 2A, while the maximum voltage is 60 V for the first output channel and 30 V for the second one.

Each FBG is accompanied by a *SHT85 sensor* which simultaneously acquires the local value of the ambient temperature and humidity (thus providing an indication of the actual conditions to which the FBGs are subjected). This sensor has an operating temperature range between -40 and +105 °C and measures relative humidity values from 0% to 100%. The nominal accuracy of the SHT85 sensor is equal to $\pm 1.5\%$ RH for relative humidity and ± 0.1 °C for temperature. These sensors have been set to acquire the temperature and relative humidity values for a time interval of 10 seconds at each measurement.

The *ARDUINO UNO microcontroller* is the electronic board that shall receive and communicate data acquired by SHT85 sensors. It sends information about sensors to the *Personal computer (PC)* by using a USB link. These data are saved in a MATLAB script, and they are linked to those arriving from the *SmartScan SBI* interrogator about the FBG response.

3.1. About measured experimental data

As shown in figure 1, three subsystems have been created to carry out a preliminary analysis by testing different temperature and humidity regimes in diverse test conditions. The first test equipment, called "Fridge", was placed in a refrigerated environment characterized by shallow temperature and humidity excursions; it has a thermic range of about 2 °C (nominally from -1 to +1 °C). A second device, called "Table", is positioned directly inside the laboratory and, therefore, measures the environmental test conditions (linked to the evolution of the weather and other anthropogenic effects). On the contrary, the third subsystem, called "Radiator", was placed near a convector (used for heating one of the laboratory rooms) to be subject to periodic and significant variations in temperature and ambient humidity.

The test bench gives as output a file containing the values measured by the FBG (in terms of reflected wavelength) and the SHT85 (temperature and humidity). In the "Fridge" the outputs are really constant for all the four periods considered, with a thermic excursion of about 2 °C, from ≈ -1 °C to $\approx +1$ °C. The trends present really frequent oscillations between these two extremes. On the contrary, "Radiator" puts in evidence a significant thermic excursion of about 20 °C with an easy understandable daily cyclic trend. Indeed, the curves show a temperature of about 20°C when the heating is switched off and values around +40°C when the system works during the day. The "Table" subsystem acquires trends that are similar to the radiator but with different absolute values. Indeed, also on the table the daily thermic excursion is detected and obviously it is linked to the heating, but with a lower thermic excursion (not over 10 °C). It should be noted that, in the periods in which the heating system is off, the environmental conditions measured by the sensors positioned on the "Radiator" station are almost coincident with those detected by the "Table".

Concerning the relative humidity measured by the SHT85 sensors, trends related to the measurement station considered and the environmental conditions (alternation day-night, weather conditions, etc.) were found. Anyway, the presence of relevant variations of relative humidity will be useful for the next step of the analyses, in order to quantify its effects on the FBG's output.

Therefore, it is now possible to analyze the FBGs outputs and their correlation with environmental conditions. For example, we will consider below the trend of the measurements carried out on the "Radiator" station over a month (from 07 January to 07 February 2020).

It is clear that, while not directly modifying the initial deformation of the fiber (due to a first adjustment of the micro-manipulator, which are then blocked), a variation in wavelength is nevertheless detected. The trend of this wavelength variation $\Delta\lambda_B$, acquired by the FBG (fig. 2), shows evident correlations with the local temperature variation (fig. 3), measured by the SHT85 sensor.

The correlation between the wavelength variation reported by the FBG and the local temperature trend is even more evident by comparing in detail the curves shown in Figures 2 and 3 by considering their daily trends. For this purpose, figures 4 and 5 respectively show the FBG wavelength trends (fig. 4) and the local temperature (fig. 5) acquired over a whole day (January 10, 2020).

As previously reported, the SHT85 probes also measured the relative humidity to analyze its temporal evolution, look for any correlations with the wavelength acquired from the FBGs, and, if necessary, implement an appropriate compensation strategy. An example of a temporal trend of relative humidity, referring to the same sampling day considered for the graphs of figures 4 and 5, is shown in figure 6. Humidity, obviously linked to environmental conditions, is greatly affected by the influence of temperature. While varying significantly throughout the test, it does not cause macroscopic effects on the deformation acquired by the FBGs sensors.

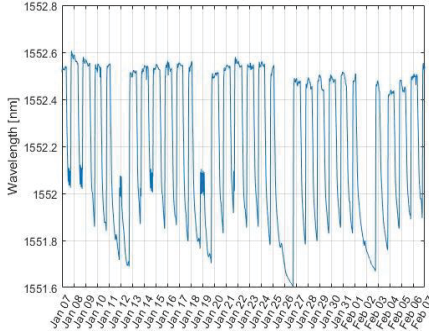


Fig. 2. Time evolution of the wavelength acquired by the FBG sensor of the "Radiator" test equipment (07/01/2020-07/02/2020).

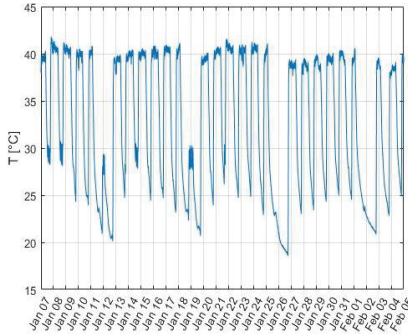


Fig. 3. Time evolution of the local temperature acquired by the SHT85 of the "Radiator" equipment (07/01/2020-07/02/2020).

4. Data analysis

The analysis is carried out on the results provided by the experimental test bench. All the post processing have been performed by means of MATLAB algorithms specifically created for this purpose. These algorithms filter the signals of the SHT85 sensor (to eliminate its signal noise) and synchronize, sub-sample, and average the data acquired to obtain a coherent and comparable data matrix.

In this way, it is possible to directly evaluate the correlation between temperature and wavelength already noticed, observing the general data collected by the test bench. In particular, as illustrated in figure 7, we can evaluate the $w(T)$ curve, which represents the variation of the wavelength acquired by FBGs as a function of the corresponding temperature. Once the curve has been plotted, the following step is to calculate the equation of the $w(T)$ linear interpolation. Therefore, it will be possible to subtract the temperature contribution from the overall FBG output. The linear fit is calculated through the least-squares method already implemented in the MATLAB functions library. The so obtained angular coefficient of the linear interpolation can (partially) correct the previously measured wavelengths, filtering disturbances due to the temperature's influence.

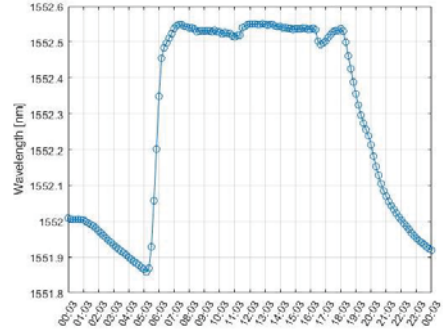


Fig. 4. Time evolution of the wavelength acquired in a whole day by the FBG sensor of the "Radiator" test equipment (10/01/2020).

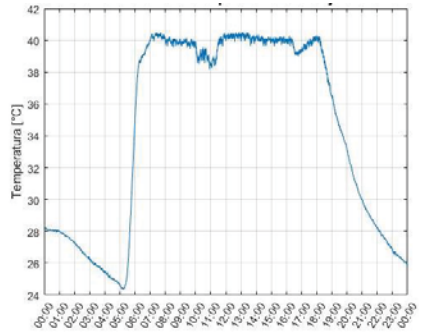


Fig. 5. Time evolution of the temperature acquired in a whole day by the SHT85 sensor of the "Radiator" equipment (07/01/2020).

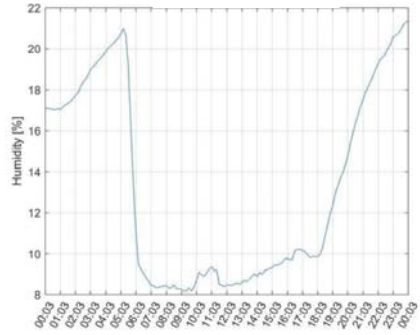


Fig. 6. Time evolution of the relative humidity acquired in a whole day by the SHT85 sensor of the "Radiator" (07/01/2020).

To this purpose, the following relation is applied:

$$\lambda_i = \lambda_{i_sist} - c_t \Delta T \tag{6}$$

where:

- λ_{i_sist} is the FBG's output measured by the test-bench;
- c_t is the angular coefficient of the linear fit for the $w(T)$ curve;
- ΔT is the temperature's variation.

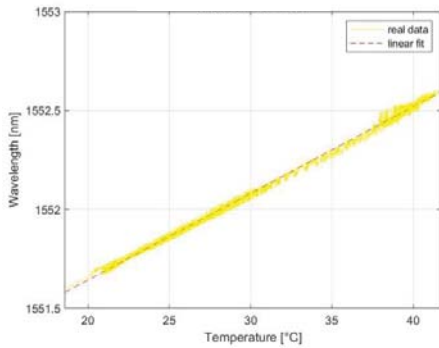


Fig. 7. $w(T)$ curve related to the "Radiator" test equipment.

Note that ΔT is calculated as the difference between the temperature measured in the i^{th} instant and the first sample acquired (T_0), which is taken as reference temperature:

$$\Delta T = T_i - T_0 \quad (7)$$

Therefore, based on the previous considerations and equations 6 and 7, we can filter the effects produced on the wavelength acquired by the temperature variations, obtaining a new curve named "*FBG – T filtered*".

The same approach can be also applied to evaluate the effects of relative humidity on the FBG measures. Therefore, we can plot a new $w(H)$ curve, representing the FBG wavelength variation as a function of corresponding humidity. We can calculate the linear fit of the $w(H)$ curve based on the same considerations previously reported. In this way, it is possible to subtract the contribution of the relative humidity from the overall results. However, regarding the humidity effects, the starting value of wavelength is not measured by the test-bench but calculated using the "*FBG – T filtered*" curve.

The so calculated wavelength values, composing a new curve called "*FBG – T-H filtered*", are filtered by most disturbances due to temperature and relative humidity. They are calculated with the following relation:

$$\lambda_i = \lambda_{it_{filt}} - c_h \Delta H \quad (8)$$

where:

- $\lambda_{it_{filt}}$ is the i^{th} value of the T filtered curve
- c_h is the angular coefficient of the linear fit for the $w(H)$ curve
- ΔH is the relative humidity variation.

ΔH is obtained as the difference between the relative humidity measured in the i^{th} instant and the first measure, that is taken as reference (H_0):

$$\Delta H = H_i - H_0 \quad (9)$$

Figure 8 represents the "*FBG – T-H filtered*" curve obtained based on the measurements acquired by the "Radiator" test equipment.

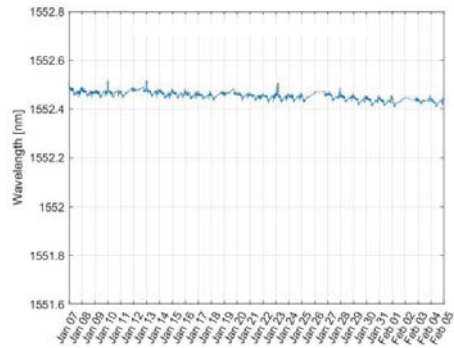


Fig. 8. *FBG – T-H filtered* curve for "Radiator" test equipment.

It is possible to evaluate the effectiveness of the proposed method by comparing the above-mentioned filtered curve with the unfiltered one reported in figure 2.

5. Conclusions

The data collected by the test bench appear to be consistent with each other and in line with the expected results. Furthermore, given that our experimental campaign lasted four months, the system has shown that it can operate autonomously for extended time intervals, guaranteeing a satisfactory level of reliability. Considering the results given by the analysis, the most important observation is about the relevant dependency of the FBG output from the environmental conditions. Indeed, the temperature resulted as the most influencing parameter on wavelength trends.

This relation has been demonstrated in chapter 4, plotting the $w(T)$ curves and calculating the linear fit of the experimental data. So, the consequence is that when FBG sensors are employed to quantify the mechanical strains, the uncertainty of the results rises with increasing thermal excursion if data are not compensated. On the contrary, once the wavelength trend is filtered from the contribution of the environmental conditions, the so obtained results put in evidence only slight oscillations, fundamentally due to negligible values of uncertainty on the strain calculate.

In conclusion, optical fiber technology and FBGs can find promising applications in aerospace sensors, particularly for the advantages in terms of costs, weight, and immunity to electromagnetic waves.

However, especially for their application as structural sensors (strain, stress, vibration, etc.), it resulted fundamental to define a straightforward and reliable process of thermal compensation. Indeed, in several aerospace applications, the values of thermal excursion can be very relevant (influencing the corresponding FBGs strain measurements). Still, the stringent constraints of safety impose to filter the thermal disturbances to have reliable and precise measures.

Acknowledgement

This work was developed within the research activity promoted by PhotoNext (<http://www.photonext.polito.it>), the Inter-Departmental Center for Photonic technologies of the Politecnico di Torino. The authors also wish to thank the LINKS laboratory for their precious assistance to the experimental activities presented in this paper.

References

- Adamovsky, G., S.F. Lyuksyutov, J.R. Mackey, B.M. Floyd, U. Abeywickrema, I. Fedin and M. Rackaitis (2012). Peculiarities of thermo-optic coefficient under different temperature regimes in optical fibers containing fiber bragg gratings. *Optics Communications* 285(5), 766 – 773.
- Ahuja, D. and D. Parande (2012). Optical sensors and their applications. *J. of Scientific Research and Reviews* 1(5).
- Anderson, R.J. and S.R. Aylward (1993). Lab Testing of Neural Networks for Improved Aircraft Onboard-Diagnostics on Flight-Ready Hardware. *Annual Reliability and Maintainability Symposium*.
- Berri, P.C., M.D.L. Dalla Vedova and L. Mainini (2018). Diagnostics of Actuation System Faults from Dynamic Data. *6th European Conference on Computational Mechanics (ECCM 6)*.
- Berri, P.C., M.D.L. Dalla Vedova and L. Mainini (2019a). Real-time Fault Detection and Prognostics for Aircraft Actuation Systems. *AIAA SciTech Forum*, AIAA 2019-2210.
- Berri, P.C., M.D.L. Dalla Vedova, P. Maggiore and T. Sclopito (2019b). Feasibility study of FBG-based sensors for prognostics in aerospace applications. *Journal of Physics: Conference Series* 1249, 012015.
- Borello, L., M.D.L. Dalla Vedova, G. Jacazio and M. Sorli (2009). A Prognostic Model for Electrohydraulic Servovalves. *Proc. of the 2009 Annual Conference of the Prognostics and Health Management Society (PHM 2009)*.
- Brusa, E., M.D.L. Dalla Vedova, L. Giorio and P. Maggiore (2019). Thermal condition monitoring of large smart bearing through fiber optic sensors. *Mechanics of Advanced Materials and Structures*, pp. 1-7.
- Byington, C.S., W. Watson, D. Edwards and P. Stoelting (2004). A Model-Based Approach to Prognostics and Health Management for Flight Control Actuators. *IEEE Aerospace Conference Proceedings*, Big Sky, USA.
- Dalla Vedova, M.D.L., P.C. Berri and S. Re (2019). Novel Metaheuristic Bio-Inspired Algorithms for Prognostics of Onboard Electromechanical Actuators. *International Journal of Mechanics and Control* 19(2), 95-101.
- De Martin, A., M. Sorli and G. Jacazio (2019). Integrated Health Monitoring for Robust Actuation System of UAV Primary Flight Controls. *International Journal of Mechanics and Control* 20(2).
- Goebel, K., M.J. Daigle, A. Saxena, I. Roychoudhury, J.R. Celaya and S. Sankararaman (2017). *Prognostics: The Science of Making Predictions*. Createspace Independent Publishing.
- Hasan, A. and T.A. Johansen (2018). Model-Based Actuator Fault Diagnosis in Multirotor UAVs. *International Conference on Unmanned Aircraft Systems*.
- Jones, K. (2018). *Temperature compensation of FBG strain sensors*. Smart Fibres Ltd, Notes 04.
- Kashyap, R.(2010). *Fiber Bragg Gratings. Optics and Photonics*. Elsevier.
- Kreuzer, M. (2006). *Strain measurement with fiber bragg grating sensors*. HBM.
- Krohn, D.A., T. MacDougall and A. Mendez (2014). *Fiber optic sensors: fundamentals and applications*. SPIE Press.
- Lelli, A. (2020). *Design and Development of a Test Bench for the Study of Temperature and Humidity Effects on Optic Sensors*. Bachelor of Science Thesis, Politecnico di Torino.
- Mihailov, S.J. (2012). Fiber Bragg grating sensors for harsh environments. *Sensors* 12(2), 1898-1918.
- Mihailov, S.J., D. Grobncic, C. Hnatovsky, R.B. Walker, P. Lu, D. Coulas and H. Ding (2017). Extreme Environment Sensing Using Femtosecond Laser-Inscribed Fiber Bragg Gratings. *MDPI Sensors* 17(12), 2909.
- Ramakrishnan, M., G. Rajan, Y. Semenova, and G. Farrell (2016). Overview of fibre optic sensor technologies for strain/temperature sensing applications in composite materials. *Sensors* 16(1)
- Santos, J.L. and F. Farahi (2018). *Handbook of Optical Sensors*, CRC Press.
- Tanaka, N., Y. Okabe and N. Takeda (2003). Temperature-compensated strain measurement using Fiber Bragg Gratings sensors embedded in composite laminates. *Smart Materials & Structures* 12(6), 940-946.
- Quattrocchi, G., P.C. Berri, M.D.L. Dalla Vedova and P. Maggiore (2020). Innovative actuator fault identification based on back electromotive force reconstruction. *Actuators* 9(3), 50.
- Quattrocchi, G., P.C. Berri, M.D.L. Dalla Vedova and P. Maggiore (2021). Optical fibers applied to aerospace systems prognostics: Design and development of new FBG-based vibration sensors. *IOP Conference Series: Materials Science and Engineering* 1024(1), 012095.
- Vachtsevanos, G., F. Lewis, M. Roemer, A. Hess and B. Wu (2006). *Intelligent Fault Diagnosis and Prognosis for Engineering Systems*. Wiley.
- Wang, W., Y. Yu, Y. Geng and X. Li (2015). Measurements of thermo-optic coefficient of standard single mode fiber under large temperature range. *Proc. SPIE* 9620, 2015 Int. Conf. Optical Instruments and Technology.